DEPARTMENT OF PHYSICS
COLLEGE OF SCIENCES
OLD DOMINION UNIVERSITY
NORFOLK, VIRGINIA 23529

SDIO/IST ULTRASHORT WAVELENGTH LASER

"Novel Experimental Schemes for Observing the Mossbauer Effect in Long-Lived, Nuclear Levels and Nuclear Coherent States"

By

Gilbert R. Hoy, Principal Investigator

Report #2
For the period May 27, 1988 through February 27, 1989

Prepared for
Naval Research Laboratory
4555 Overlook Ave., SW
Washington, D.C. 20375-5000
Attn: Code 4720

Under
Research Contract N00014-87-K-2015
Dr. P. Kepple, Scientific Officer

Submitted by the
Old Dominion University Research Foundation
P. O. Box 6369
Norfolk, Virginia 23508

March 1989

SDIO/IST ULTRASHORT WAVELENGTH LASER

REPORT#2

"Novel Experimental Schemes for Observing the Mössbauer Effect in Long-Lived, Nuclear Levels and Nuclear Coherent States"

by

Gilbert R. Hoy

General Remarks

Our new Gamma-Ray Optics Laboratory is now fully functional. At the present time there are three Ph. D. students working in the laboratory. Shokrollah Rezaie-Serej is deeply involved in his dissertation "Search for the Mössbauer Effect in ^{109}Ag". The two other students, Hsing-Ching Chang and Jialin Zeng, are just begining there research. Their subject areas will be "Conversion-Electron, Position-Sensitive Detection," and "Gamma-Ray Optical Studies of Multibeam Borrmann Modes," respectively. Professor F. P. Clay Jr. (Old Dominion University, Physics Department) has also joined our effort. Prof. Clay is an expert in electronic and vacuum physics. His advice and council will be most helpful. We continue our important collaboration with Dr. R. Dean Taylor (Los Alamos National Laboratory) on problems of mutual interest.

Mössbauer Effect in Long-lived Nuclear Levels (^{109}Ag) (with Shokrollah Rezaie-Serej)

There are several aspects of the single-crystal, self-absorption, source technique that have needed further analysis (Refs. 1,2). In this report we will explain our calculational study designed to improve our

theoretical model by incorporating a gaussian, source distribution and including solid angle effects.

Our current experiments have been done in the vertical geometry. i.e. the single crystal is lying flat and the Ge detector is positioned below. In this configuration there are two solid angle effects: not only the fact that different sample slices subtend slightly different solid angles at the detector, but also the fact that, due to the contraction of the dewar-sample system itself, an overall temperature dependent solid angle effect is produced.

Source Distribution

We assume that the distribution of the source nuclei, ^{109}Cd, in the silver sample follows the usual gaussian distribution (Ref. 3) as shown in Eq. (1). The value of α depends on the diffusion constant for ^{109}Cd in silver, and the temperature and time of the anneal.

$$C(x) = C_0 \, e^{-\alpha x^2} \qquad (1)$$

where C_0 is the source density per unit length

Solid Angle Effects

Figure 1 shows a schematic representation of the sample-holder, sample, detector assembly. The radius of the cylindrical detector is a and the radius of the cylindrical sample is represented by b. The geometrical, solid-angle factor for a particular sample slice located by x in Figure 1 is given by (Ref. 4) Eq. (2) below, where we have only kept the first two terms. Notice that z_0, and hence z, are temperature dependent.

$$G(z) = \frac{1}{2}\left[1 - \frac{z}{(z^2 + a^2)^{1/2}} \right] - \frac{3}{16} \frac{b^2 a^2 z}{(z^2 + a^2)^{5/2}} + \ldots \qquad (2)$$

where $z = z_0 - x$.

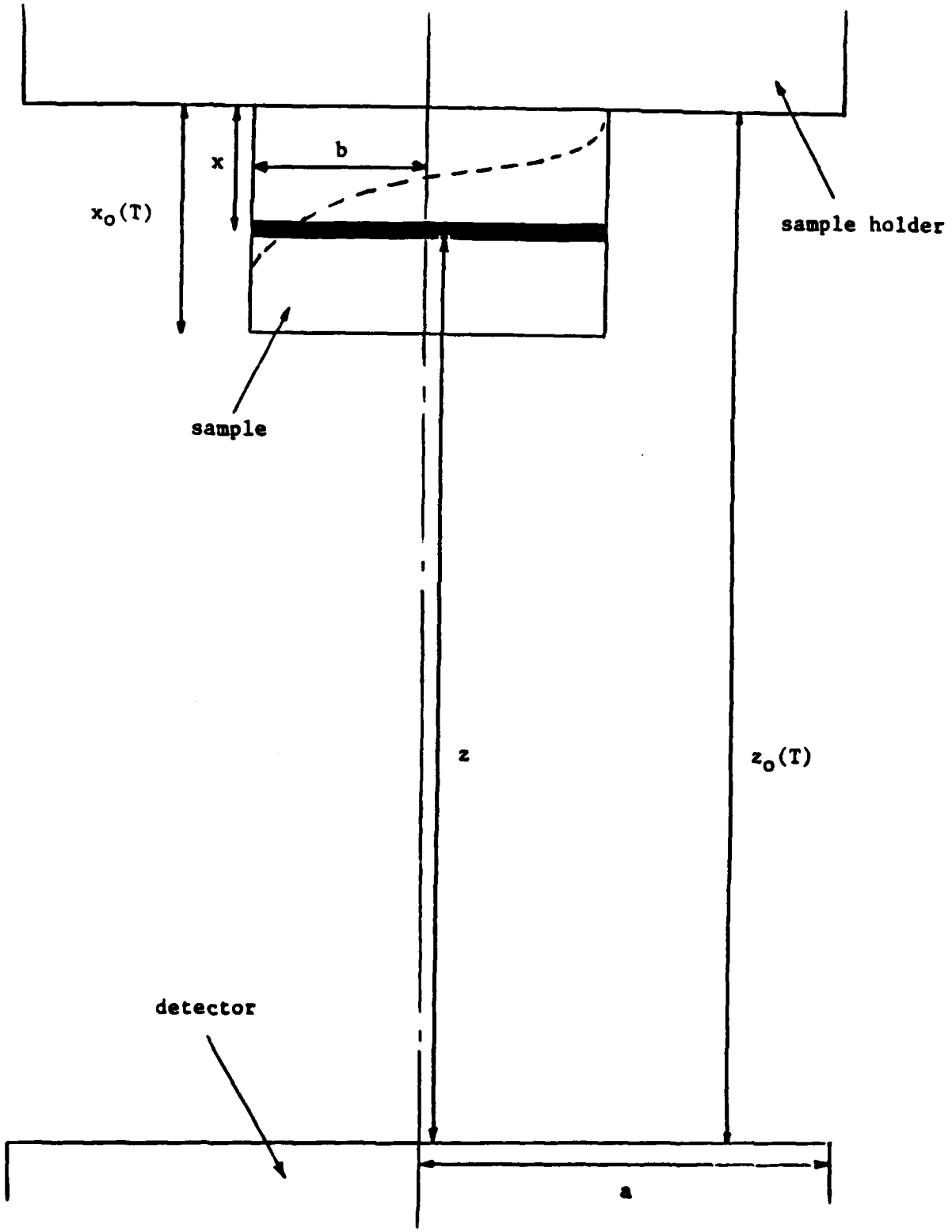

Fig. 1. A schematic represention of the experimental configuration. Notice the temperature dependence of z_o and x_o due to the contraction of the materials as the temperature is lowered. The solid angle subtended by the detector is thus temperature dependent.

Theoretical Model

In general, the intensity of radiation reaching the detector from the sample is obtained using Eqs. (1) and (2) and summing over the contributions from all sample slices. Eq.(3) shows the result where: G(z), expressed as a function of x, is the geometrical, solid-angle factor, μ is the absorption coefficient (mass absorption coefficient times the density), λ is the source decay constant, and x_o is the sample thickness.

$$I = C_o \lambda e^{-\mu x_o - \lambda t} \int_o^{x_o} G(x) e^{-\alpha x^{\cos}} + \mu x \, dx \qquad (3)$$

where C_o, x_o, G(x), and μ are temperature dependent.

The intensity of the radiation reaching the detector due to the 22-keV, K_α x-ray is given by Eq. (4). The parameters take on the appropriate values for 22-keV radiation and the fact that the sample is silver.

$$I_{K_\alpha} = C_{K\alpha} C_o \lambda e^{-\mu_{K\alpha} x_o - \lambda t} \int_o^{x_o} G(x) e^{-\alpha x^{\cos} + \mu_{K\alpha} x} \, dx \qquad (4)$$

where $C_{K\alpha}$ is a constant.

There is a similar expression, Eq. (5), which expresses the result for the 88-keV, gamma radiation. In this case, there is an additional factor associated with the possible occurrence of nuclear, gamma-ray, resonance absorption i.e. the Mössbauer effect.

$$I_\gamma = C_\gamma C_o \lambda e^{-\mu_\gamma x_o - \lambda t} \int_o^{x_o} G(x) e^{-\alpha x^{\cos} + \mu_\gamma x} \, dx \left[(1-f) + f e^{-\mu_N x_N} \right] \qquad (5)$$

where: C_γ is a constant, μ_N is the nuclear-resonant, absorption coefficient evaluated on resonance, x_N is the effective, Mössbauer, thickness parameter, and f is the recoilless fraction.

Keep in mind that in Eqs. (4) and (5), C_o, $\mu_{K\alpha}$, μ_γ, μ_N, f, x_o, and $G(x)$ are all temperature dependent.

If one considers the ratio of the number of 22-keV, K_α x rays to the number of 88-keV, gamma rays, Eq. (6), some factors in Eqs. (4) and (5) cancel out. Fig. 2 illustrates the behavier of the ratio as a function of temperature for different source-distribution parameters α. It is of some interest to note that the dependence on α may not be quite what one would expect. At any particular temperature, the ratio as a function of α shows a minimum. This behavier at 300 K is shown in Fig. 3.

$$R_{K_\alpha \gamma} = \frac{I_{K_\alpha}}{I_\gamma} \qquad (6)$$

Experimental Results and Analysis

Our experimental procedure has included recording the number of 22-keV, K_α, x-ray and 88-keV, gamma-ray counts reaching the detector as a function of time. These data were recorded over a five-week period and the results are shown in Fig. 4. A standard procedure was adopted for collecting the data. Each run started at the same time of the day, and lasted 22 hours. In order to keep the geometrical, solid-angle factor the same for the runs at a particular temperature, special care was needed. For the runs at liquid nitrogen and helium temperatures, the levels of the cryogenic fluids where initially set at specific values and maintained so as to insure that the geometrical, solid-angle factor remained the same for all runs at the same temperature.

These data were analyzed by using the known decay constant for ^{109}Cd and doing a least-squares analysis to determine the intercept at time $t = 0$ for each of the three lines corresponding to the results at 295 K, 78 K and

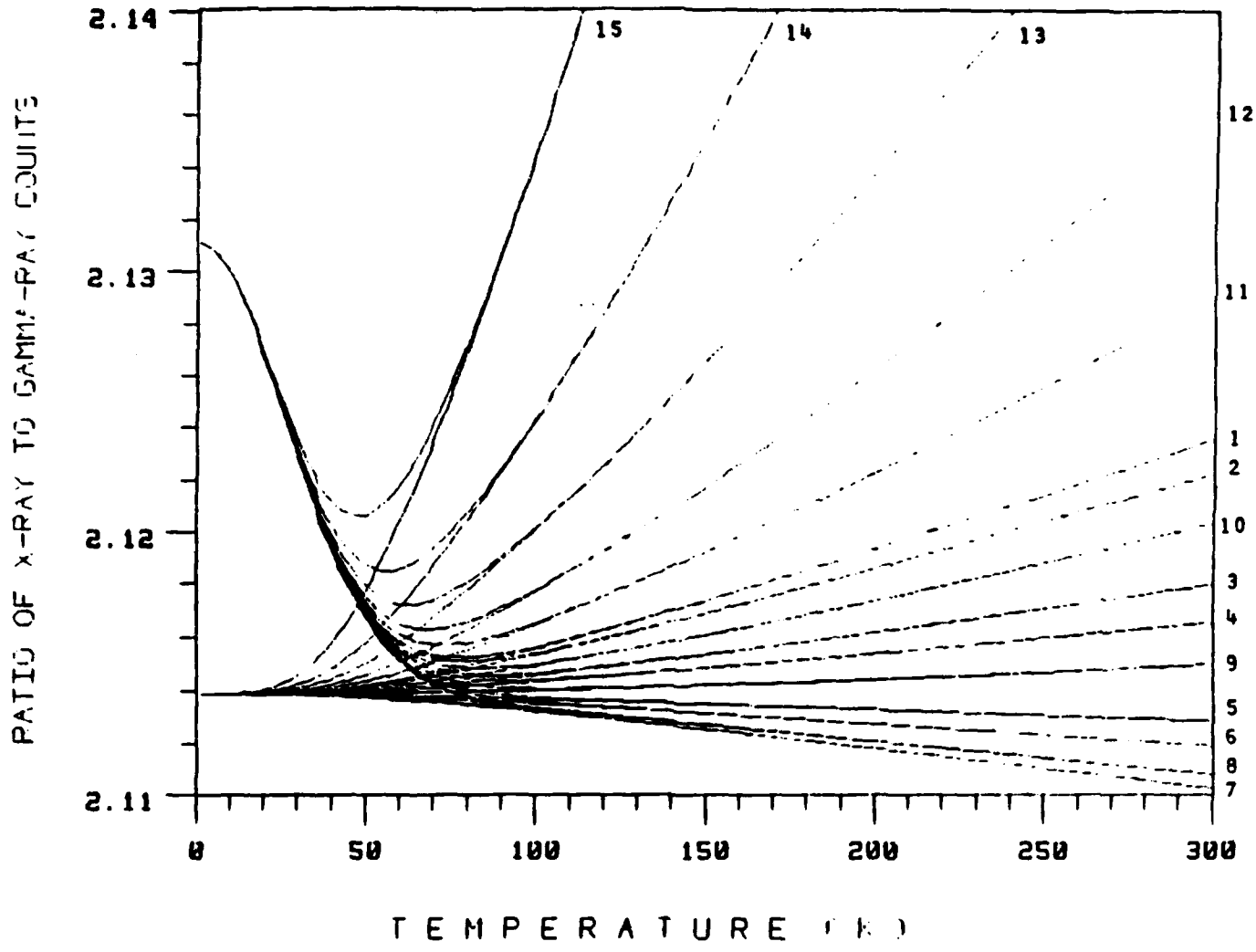

Fig. 2. The theoretical results for the ratio of 22-keV, x-ray to 88-keV, gamma-ray counts are shown as a function of temperature according to the formulation described in the text. In addition, curves are plotted for different values of the source-distribution parameter α as indicated by the numbers on the top and right side of the figure. The numbers 1, 2, 3,...etc. correspond to α values of 0, 100, 400, 500, 800, 900, 1200, 1500, 1900, 2200, 2600, 2900, 3500, 5000, and 100 000 cm^{-2}, respectively. The curves that go up on the left hand side correspond to an assumed Mössbauer effect corresponding to an effective, Mössbauer, thickness parameter $x_M = 0.24 \times 10^{-2}$ cm. The curves that stay down on the left hand side correspond to zero Mössbauer effect.

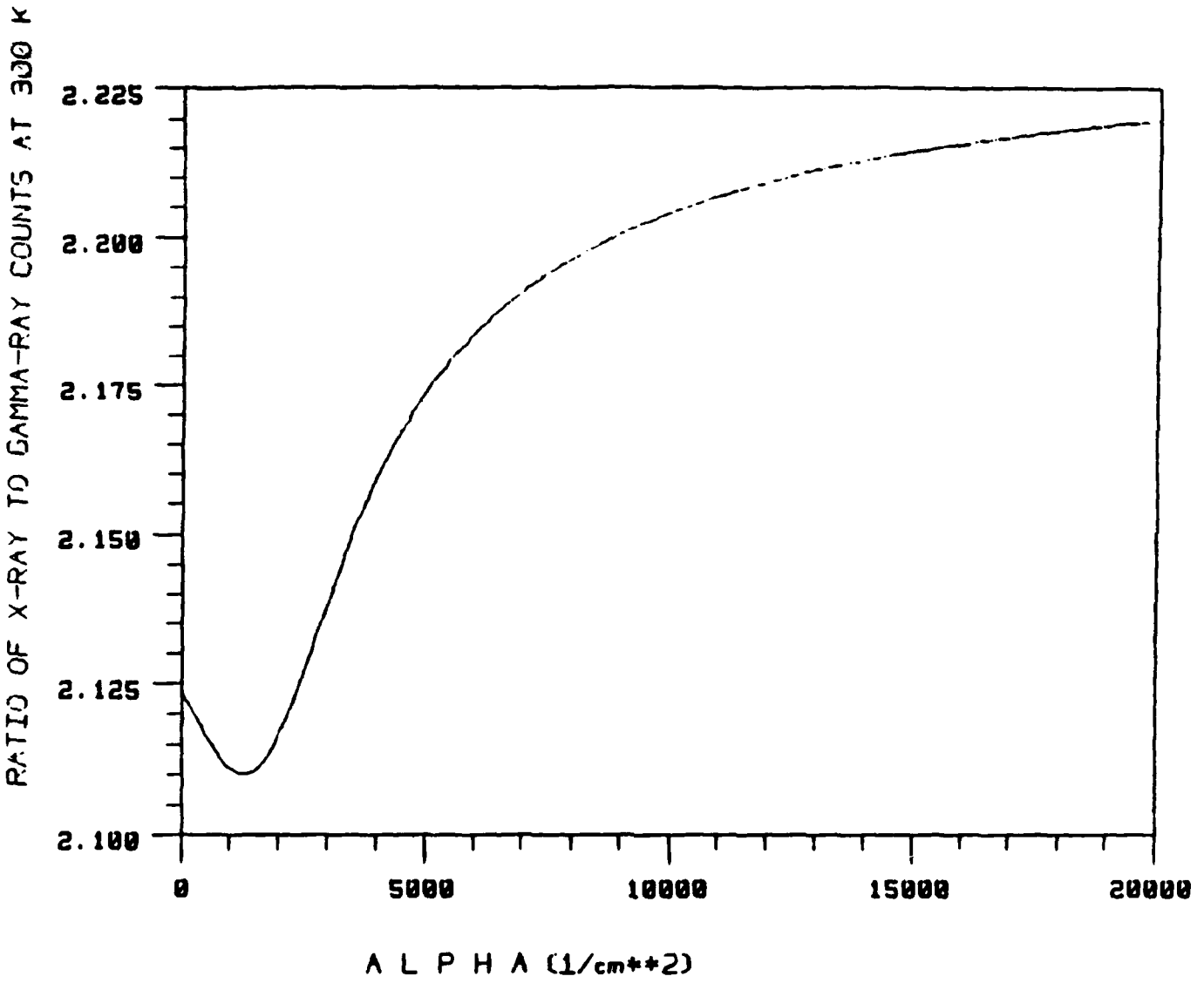

Fig. 3. The theoretical results for the ratio of 22-keV, x-ray to 88-keV, gamma-ray counts for our system, when the sample is at 300 K, are shown as a function of the source-distribution parameter α. These result are normalized to a particular value at 1 K. Notice how the result shows a minimum for a particular α value. This behavior is the result of the normalization procedure.

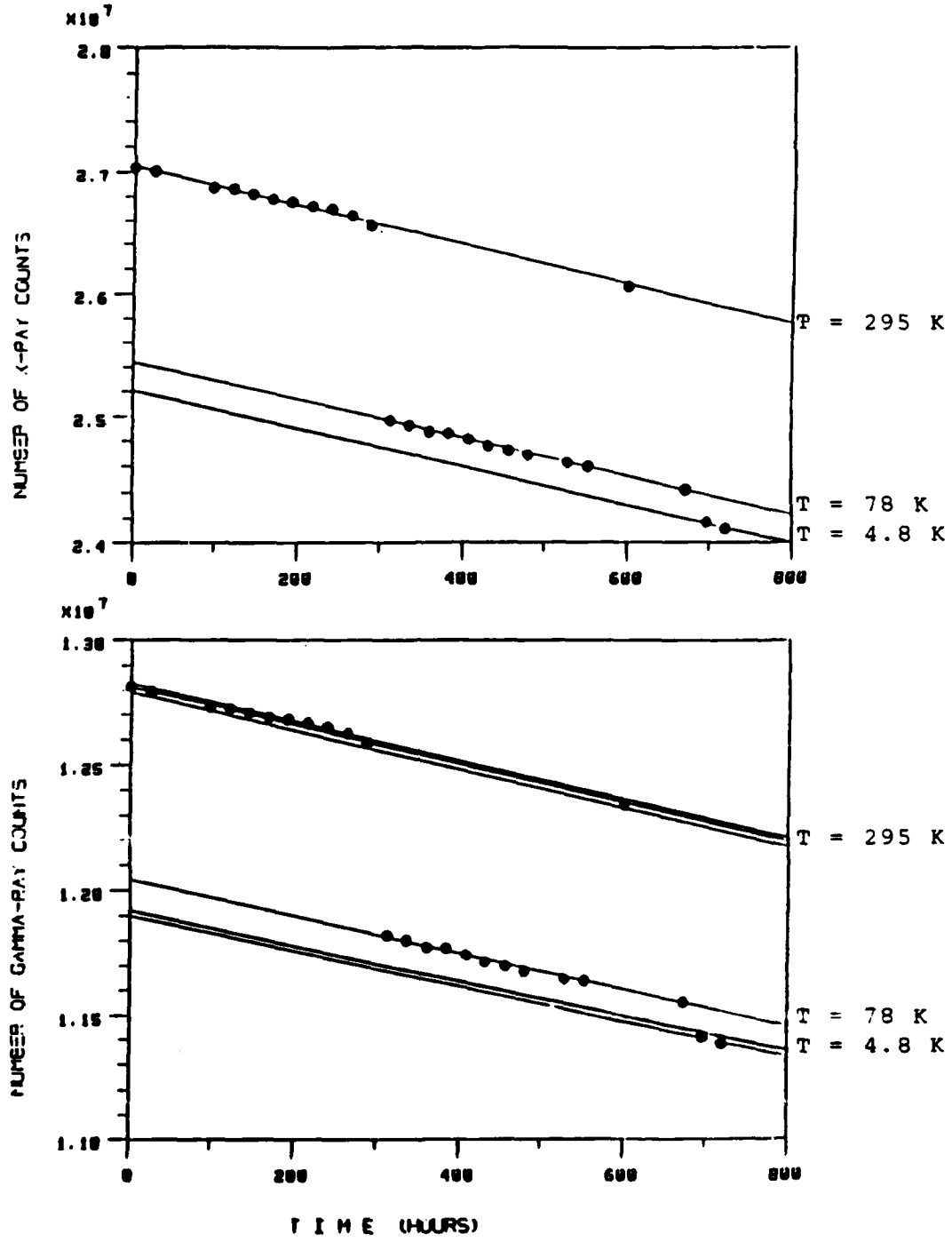

Fig. 4. The top half of the figure shows our experimental data for the counting rate of the 22-keV x rays as a function of time with the sample at three different temperatures. The three solid lines are obtained by a least squares fitting procedure in which the known decay constant for ^{109}Cd is used. The drop in the data at lower temperatures is due to thermal contraction and the geometrical solid-angle effects. These factors are determined by fitting these data. In the lower half of the figure, similar data for the 88-keV gamma rays are recorded. The three parallel lines in the top half of this section correspond to the theoretical results at the three temperatures excluding the geometrical, solid-angle contribution. The two parallel lines at the bottom show the effect with and without Mössbauer absorption. The value obtained from this procedure for the effective, Mössbauer, thickness parameter x_N is 0.52×10^{-3} cm, and we set the source-distribution parameter α at 1080 cm^{-3}.

4.8 K. The values for the intercepts from the x-ray and gamma-ray data were used to determine the ratio of x-ray to gamma-ray counts at 295 K, 78 K, and 4.8K. These results are shown in Fig. 5. A nonlinear, least-squares, fitting routine incorporating our full theoretical model was used to fit Eq. (6) to the data. This gave a value of 0.48×10^{-3} cm for the effective, Mössbauer, thickness parameter and a value of 1080 cm^{-2} for the source-distribution parameter α.

Furthermore, in order to check the consistency of the technique, we fitted Eqs. (4) and (5) to the intercepts from the x-ray and gamma-ray data (see Fig. 2). First Eq. (4) was fitted to the x-ray data to determine the geometrical, solid-angle factor associated with the contraction of the dewar-sample system at liquid nitrogen and helium temperatures. (The value of the source-distribution parameter α obtained from fitting the ratio data was used here). Next the geometrical, solid-angle factor determined from fitting the x-ray data was used to fit Eq. (5) to the gamma-ray data. This procedure yielded a value of 0.52×10^{-3} cm for the effective, Mössbauer thickness, which is in good agreement with the value obtained from fitting the ratio data.

Previous research to observe the Mössbauer effect in ^{107}Ag (Ref. 5) used the same self-absorption approach. However, they recorded only the number of 88-keV, gamma-ray counts as a function of time at different temperatures. Our analysis clearly shows that in the vertical geometry, the geometrical, solid-angle effects are very significant. Our x-ray data and analysis provide the needed geometrical, solid-angle information required to successfully analyze the gamma-ray data. In the ratio technique (see Fig. 5 and Ref. 1) the geometrical, solid-angle factors essentially cancel out as does the time dependence. However, we have found

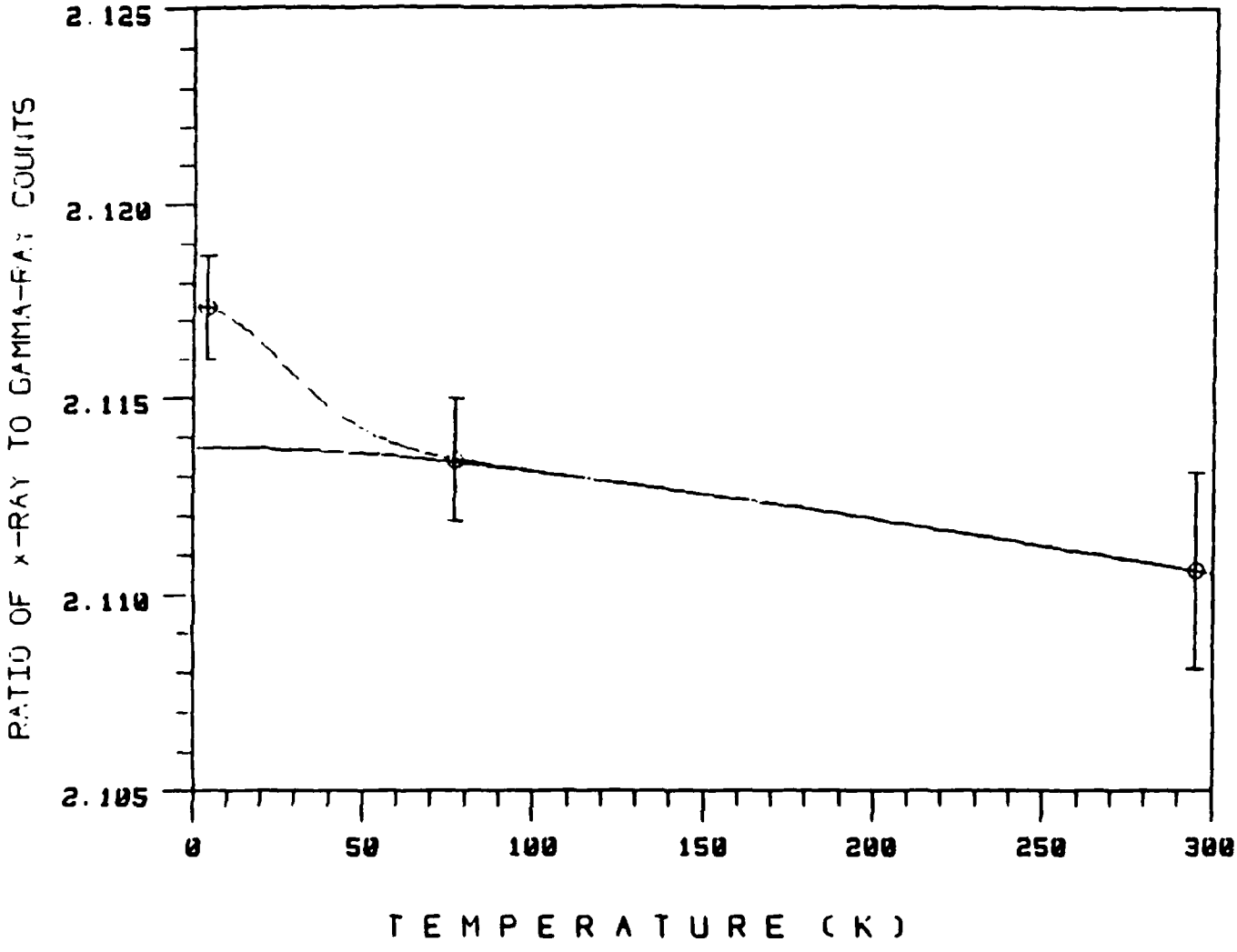

Fig. 5. Our experimental results for the ratio of 22-keV, x-ray to 88-keV, gamma-ray counts at three temperatures namely 4.8 K, 78 K and 295 K are indicated by the symbols. The two solid curves show our theoretical analysis. The lower one on the left is obtained by putting the Mössbauer effect equal to zero. The higher one includes the presence of the Mössbauer effect. Of course, both curves merge into one at higher temperatures as the Mössbauer effect goes to zero. Normalizing our experimental data and theoretical analysis to the lowest temperature value results in an effective Mössbauer thickness parameter $x_M = 0.48 \times 10^{-3}$ cm and a source-distribution parameter $\alpha = 1080\ cm^{-1}$.

that data such as that shown in Fig. 4 are very helpful in monitoring the data collection procedure and equipment stability. In fact, we were able to easily observe that after the second liquid helium run, the apparatus developed a problem.

Application of the Homogeneous Line Broadening Method for Detecting the Mössbauer Effect in ^{107}Ag

Our self-absorption, single-crystal, source method for determining the Mössbauer effect in ^{107}Ag has been described previously (Refs. 1-2). Of major concern is the possible presence of field inhomogeneities in the single crystal such that the source and absorber nuclei are in different effective fields. Because of the extreme narrowness of the 88-keV, recoilless-emission line ($\approx 10^{-17}$eV), the slightest shift between the emission profile and absorption cross section will result in no Mössbauer effect.

In general, application of an alternating, external, magnetic field on the source nuclei will produce a homogeneously-broadened, emission-line profile. Of course this procedure will also broaden the absorption cross section. For a particular degree of broadening it may be possible for the emission profile and absorption cross section to overlap and give an observable Mössbauer effect even in the presence of field inhomogeneities. In fact, this method, if successful, should produce information about the size of the inhomogeneous field effects themselves.

In order to investigate the utility of this method a Fortran computer program (SPINAG.FOR) was written for the case of ^{107}Ag. This program uses the theory formulated in a convenient form by M. Blume (Ref. 6). In this calculation an externally applied field makes stochastic fluctuations

between "up" and "down" positions. The probability of being up equals the probability of being down. The natural line width is included but the electric-field gradient is set to zero since silver is a cubic crystal. The known values of the spins, parities, and magnetic g factors for both the first excited and ground nuclear states of ^{109}Ag were used. A schematic diagram of the nuclear energy levels in the presence of an applied magnetic field is shown in Fig. 6. The relevant equation, expressing the probability that a gamma ray is emitted in direction k at frequency ω, is given by,

$$P(k,\omega)=\frac{2}{\Gamma(2I_1+1)}\,Re\int_0^{\infty} d\tau e^{i\omega\tau-(\Gamma/2)\tau}\sum_{m_0 m_1}|\langle I_0 m_0|V^+|I_1 m_1\rangle|^2(\cos x W\tau+(\sin x W\tau)/x)e^{-W\tau}$$

where,

$$x = x(m_0,m_1) = \left[\frac{(g_0 m_0 - g_1 m_1)^2\mu^2 h^2}{W^2} - 1\right]$$

In this formulation the subscript "0" refers to the ground state while the subscript "1" refers to the excited state. The parameter h is the strength of the magnetic field and W is the relaxation (or flipping) rate. Γ is the natural line width of the excited state,and another parameter θ, not shown in these equations, measures the angle between the applied magnetic field and the gamma ray observation direction. Fig. 7 a, b, and c show results for a constant, applied, magnetic field when θ equals zero, $\pi/4$, and $\pi/2$ degrees, respectively. The polarization effects associated with this E3 transition are clearly observed.

The effect on the emission profile when the magnetic field fluctuates is quite dramatic. The results of such a calculation when the magnetic field equals 30 Gauss and the relaxation rates are 0, 10 000, 100 000, 1 000 000 cycles/sec. are shown in Fig. 8. Notice that the effective width of the emission profile is relaxation rate dependent.

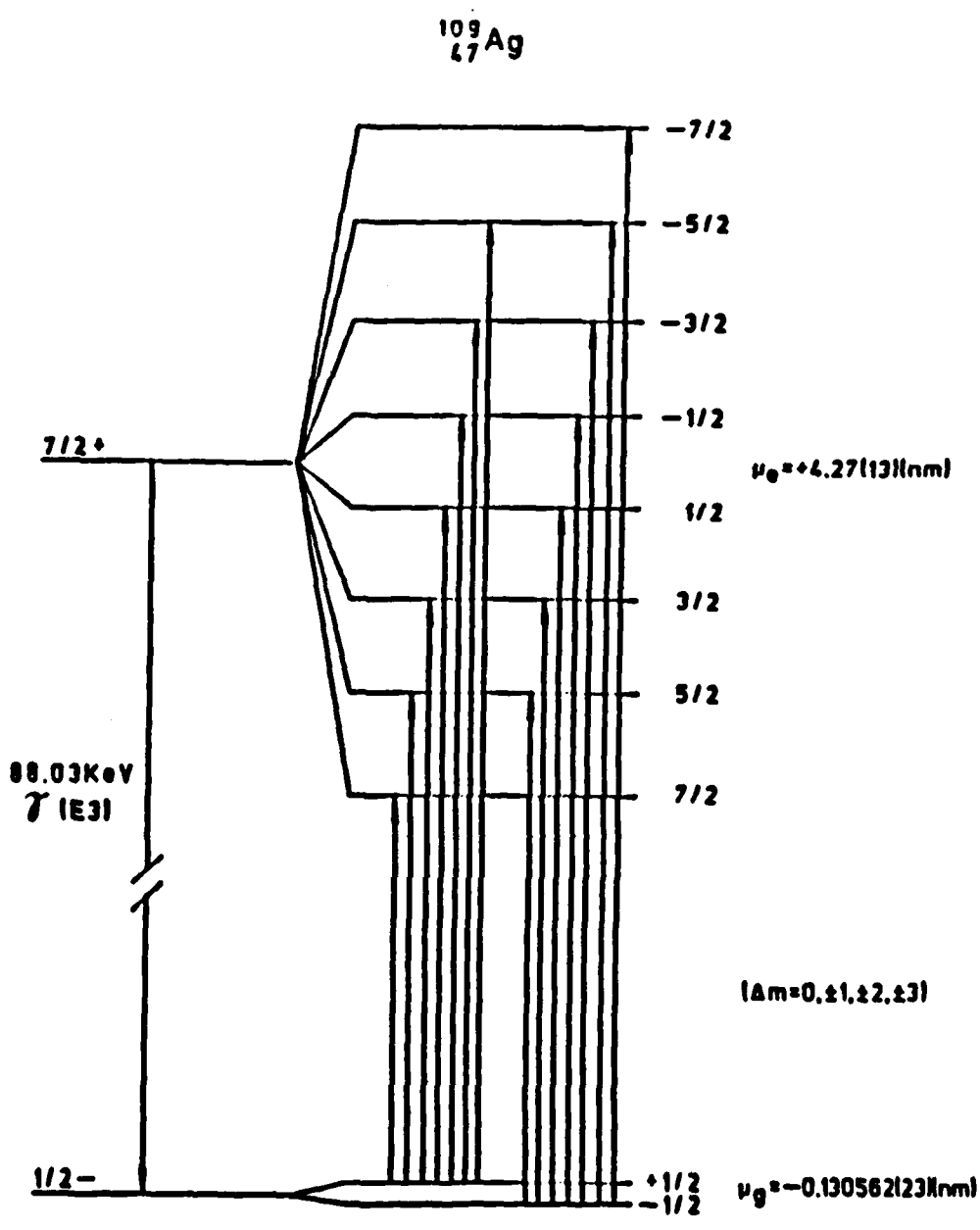

Fig. 6. The nuclear energy level diagram for the ground and first excited states of ^{109}Ag are shown in the presence of a magnetic field. Possible nuclear-resonant, absorptive transitions consistent with the E3 selection rules are also indicated.

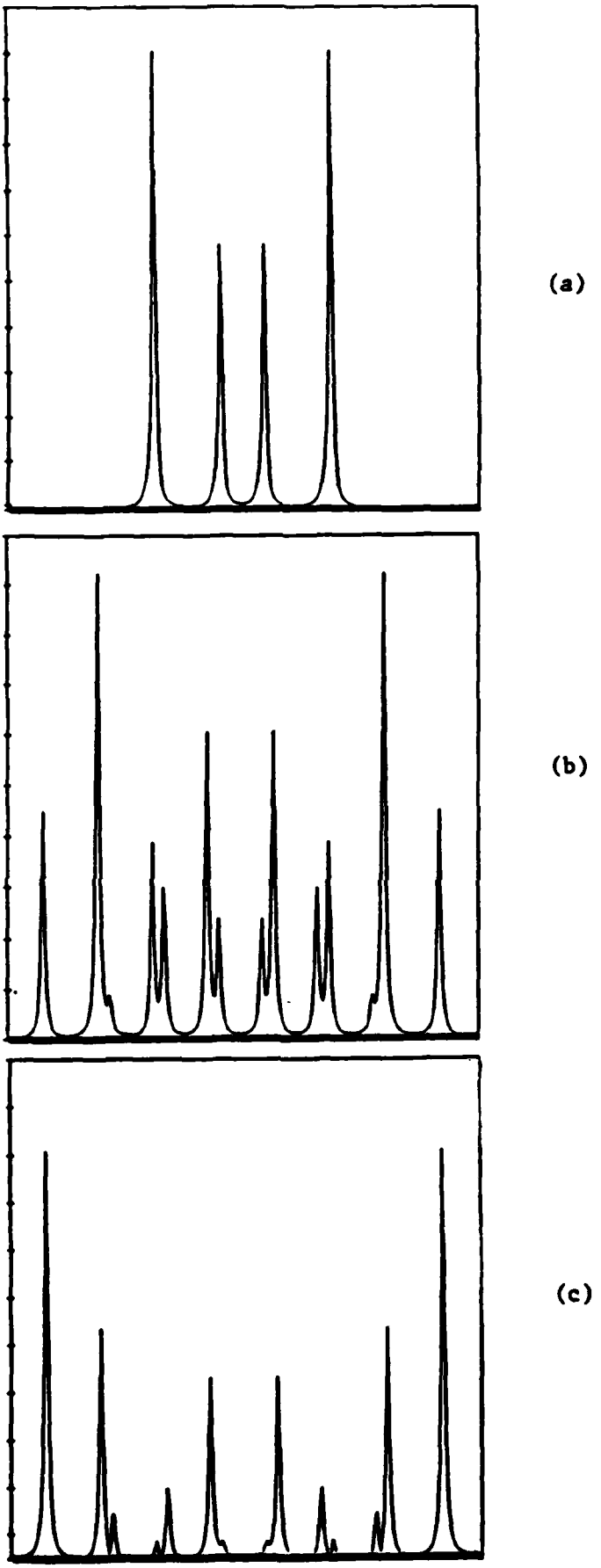

Fig. 7. The calculated Mössbauer emission spectra are shown for ^{109}Ag for three different angles θ between the applied magnetic field and the gamma ray observation direction. The value of the constant applied magnetic field is taken to be 0.36×10^{-4} gauss. The angle θ is 0, 45, and 90 degrees for a, b and c respectively.

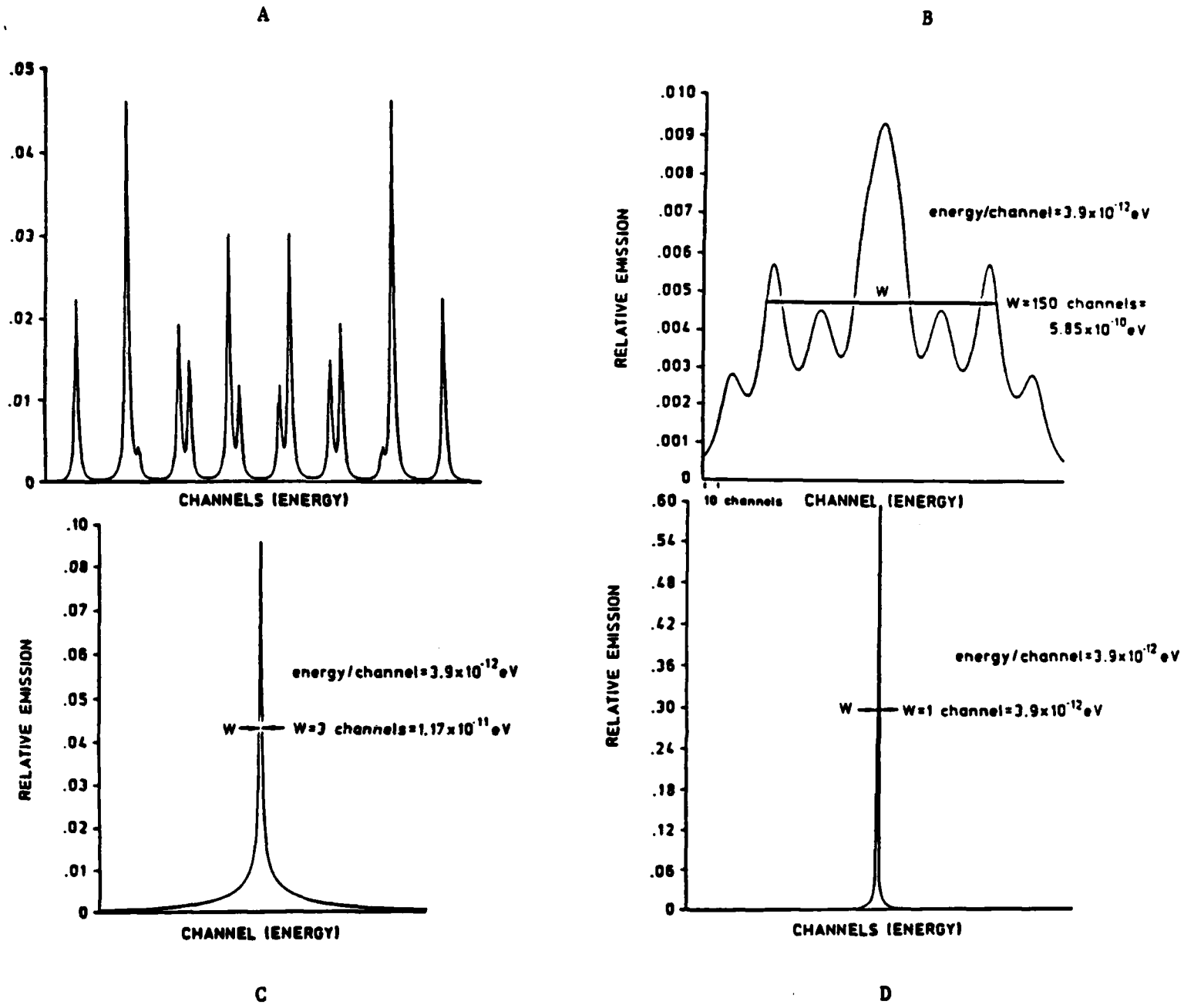

Fig. 8. The gamma-ray, emission spectrum for the case of ^{109}Ag in the presence of a fluctuating applied magnetic field is dependent on the fluctuation rate. In this example the applied magnetic field is 30 gauss and the angle θ between the applied magnetic field and the observation direction is 45 degrees. Note that the CHANNEL (ENERGY) scales are only the same for B, C and D. For cases A, B, C and D the fluctuation rates are 0, 10^{6}, 10^{8}, and 10^{9} cycles/sec respectively.

This width parameter for two magnetic field strengths is tabulated below.

Mössbauer width parameter due to a fluctuating externally applied magnetic field on a single-crystal Cd-doped sample

magnet field	energy/channel	relaxation rate	frequency	width (eV)
30 Gauss	3.9×10^{-12} eV	4×10^{-11} eV	9,800c/sec	5.8×10^{-10}
30 Gauss	3.9×10^{-12} eV	4×10^{-10} eV	98,000c/sec	1.2×10^{-11}
30 Gauss	3.9×10^{-12} eV	4×10^{-9} eV	980,000c/sec	3.9×10^{-12}
3 Gauss	3.9×10^{-13}	4×10^{-12}	980c/sec	5.8×10^{-11}
3 Gauss	3.9×10^{-13}	4×10^{-11}	9,800c/sec	1.2×10^{-12}
3 Gauss	3.9×10^{-13}	4×10^{-10}	98,000c/sec	3.9×10^{-13}

We are planning to design an experiment to explore the possibility of using this technique in the study of the Mössbauer effect in long-lived, nuclear levels.

Symmetry of Reciprocal Lattice Planes Used For Multibeam Borrmann Modes

In cubic crystals, a direction with directional indices [hkl] is normal to the plane whose Miller indices are (hkl). (This is not generally true for other crystal systems.) For this reason it is useful when referring to body centered cubic (bcc) and face centered cubic (fcc) structures to use cubic rather than primitive unit cells. The reciprocal lattice of the bcc lattice is an fcc lattice. The basis vectors of this lattice can be written in terms of the usual cubic orthonormal set by,

$$a^* = \frac{2\pi}{a}(i + j); \; b^* = \frac{2\pi}{a}(j + k); \; c^* = \frac{2\pi}{a}(i + k)$$

A vector of the reciprocal lattice can be written as,

$G = 2\pi(ha^* + kb^* + lc^*)$ or in the cubic basis,

$G = \frac{2\pi}{a}[(h + l)i + (h + k)j + (k + l)k]$ (for a bcc lattice)

In a similiar fashion , one can write the reciprocal lattice for an fcc lattice. The result is,

$G = \frac{2\pi}{a}[(h-k+l)i + (h+k-l)j + (-h+k+l)k]$ (for an fcc lattice)

If one wishes to look at the plane perpendicular to the z axis in the reciprocal lattice of a bcc crystal one simply sets k = -l in the expression for G for a bcc lattice above. The resulting array of points is shown in Fig. 9a.

One method of determining the reciprocal lattice points lying in a plane perpendicular to a particular reciprocal direction is to express the reciprocal lattice in a coordinate system in which the new z axis points along that direction. This can be accomplished by using the following rotation matrix,

$$\mathbb{R} = \begin{bmatrix} \cos\theta\cos\phi & \cos\theta\sin\phi & -\sin\theta \\ -\sin\phi & \cos\phi & 0 \\ \sin\theta\cos\phi & \sin\theta\sin\phi & \cos\theta \end{bmatrix}$$

To look at the plane perpendicular to the [111] direction in the reciprocal lattice of a bcc lattice, one rotates G to G' using $G' = \mathbb{R}G$ where for this case, $\sin\theta = 1/\sqrt{3}$ and $\sin\phi = 1/\sqrt{2}$. Setting the coefficient

of the z component in G' equal to zero gives the result. The resulting array of points in the reciprocal lattice plane whose perpendicular is in the [111] direction is given in Fig. 9a. The same approach can be used for investigating an fcc crystal. The resulting reciprocal lattice planes for fcc (100) crystals and (111) crystals are shown in Fig. 9b. From these diagrams one can calculate the multibeam Borrmann cone angles θ_B where

$$\sin\theta_B = \frac{\text{radius of the Borrmann mode circle in units of } 1/a}{(\ 1\ /\ \lambda\ )}$$

λ = wavelength of the radiation

Using the table of lattice parameters given below,

bcc crystals	
substance	cubic lattice spacing
Fe	2.87 in Angstrom units
Cr	2.88
fcc crystals	
substance	cubic lattice spacing
Pd	3.89
Rh	3.80
Ni	3.52
Ag	4.09

one can calculate the multibeam Borrmann cone angles. These results were already presented in our first progress report.

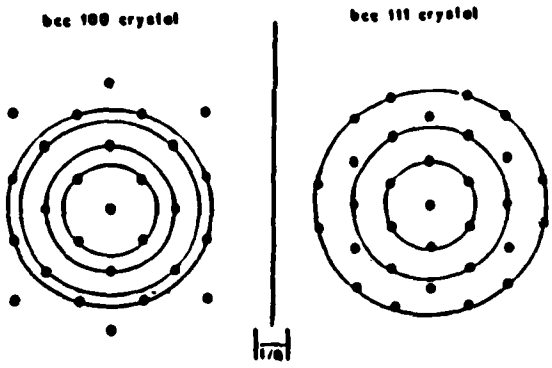

Fig. 9a. Reciprocal lattice planes perpendicular to the reciprocal lattice vectors that define the growth axis directions for (100) and (111) bcc crystals.

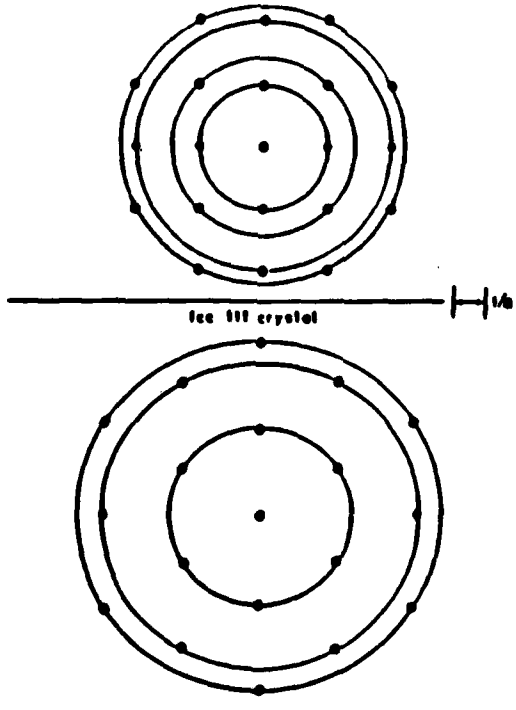

Fig. 9b. Reciprocal lattice planes perpendicular to the reciprocal lattice vectors that define the growth axis directions (100) and (111) fcc crystals.

REFERENCES

1. G.R. Hoy and R.D. Taylor, J. Quant. Spect. and Rad. Trans., 40, No. 6, 763-771, (1988).

2. R.D. Taylor and G.R. Hoy, SPIE Vol.875 "Short and Ultrashort Wavelength Lasers", January (1988).

3. J. Askill, Tracer Diffusion Data for Metals, Alloys, and Simple Oxides, (Plenum Pub. Co., New York) 1970.

4. A. H. Jaffey, Rev. Sci. Instrum. 25, 349 (1954).

5. W. Wildner and U. Gonser, J. Phys. (Paris) 40, C2-47 (1979).

6. M. Blume, in Hyperfine Structure and Nuclear Radiations, Eds. E. Matthias and D.A. Shirley (North-Holland Pub. Co., Amsterdam, 1968) pages 911 - 927.